

How to quench a galaxy

Andrew Pontzen¹, Michael Tremmel², Nina Roth¹, Hiranya V. Peiris¹,
Amélie Saintonge¹, Marta Volonteri³, Tom Quinn², Fabio Governato²

¹ *Department of Physics and Astronomy, University College London, London WC1E 6BT, UK*

² *Astronomy Department, University of Washington, Seattle, WA 98195, US*

³ *Institut d’Astrophysique de Paris, 98 bis bd Arago, 75014 Paris, France*

Received —; published—.

ABSTRACT

We show how the interplay between active galactic nuclei (AGN) and merger history determines whether a galaxy quenches star formation at high redshift. We first simulate, in a full cosmological context, a galaxy of total dynamical mass $M_{\text{vir}} = 10^{12} M_{\odot}$ at $z = 2$. Then we systematically alter the accretion history of the galaxy by minimally changing the linear overdensity in the initial conditions. This “genetic modification” approach allows the generation of three sets of Λ CDM initial conditions leading to maximum merger ratios of 1:10, 1:5 and 2:3 respectively. The changes leave the final halo mass, large scale structure and local environment unchanged, providing a controlled numerical experiment. Interaction between the AGN physics and mergers in the three cases lead respectively to a star-forming, temporarily-quenched and permanently-quenched galaxy. However the differences do not primarily lie in the black hole accretion rates, but in the kinetic effects of the merger: the galaxy is resilient against AGN feedback unless its gaseous disk is first disrupted. Typical accretion rates are comparable in the three cases, falling below $0.1 M_{\odot} \text{yr}^{-1}$, equivalent to around 2% of the Eddington rate or 10^{-3} times the pre-quenching star formation rate, in agreement with observations. This low level of black hole accretion can be sustained even when there is insufficient dense cold gas for star formation. Conversely, supernova feedback is too distributed to generate outflows in high-mass systems, and cannot maintain quenching over periods longer than the halo gas cooling time.

1 INTRODUCTION

Reproducing the population of galaxies observed in the Universe within a Λ CDM cosmological paradigm requires significant energetic feedback (White & Frenk 1991) to prevent over-cooling and excessive star formation. In fact star formation must be inefficient in both low and high mass dark matter halos, with a peak efficiency corresponding approximately to the luminosity function turnover L_{\star} (Bower et al. 2006; Guo et al. 2010; Moster et al. 2013; Behroozi et al. 2013). Regulation of galaxies with luminosities $L < L_{\star}$ can be attributed to ultraviolet background radiation slowing the accretion of gas into shallow potential wells (Efstathiou 1992; Bullock et al. 2000; Somerville 2002), and subsequently energy input from young stars (White & Rees 1978; Cole et al. 1994; Efstathiou 2000; Governato et al. 2007; Pontzen et al. 2008). The relatively shallow potential wells mean that the typical speeds achieved by supernova- and radiation-driven galactic winds can exceed the escape velocity (Mac Low & Ferrara 1999; Christensen et al. 2016). However many lines of reasoning suggest that these processes must become increasingly ineffective as dynamical masses approach $10^{12} M_{\odot}$ (Benson et al. 2003; Bower et al. 2006; Hopkins et al. 2014; Keller et al. 2016).

Accounting for reduced star formation at high masses has proved more contentious. Early scaling arguments and semi-

analytic models suggested that long cooling times associated with the raised virial shock temperature could be a simple explanation (Binney 1977; Rees & Ostriker 1977; White & Rees 1978; Kauffmann et al. 1993; Cole et al. 1994; Somerville & Primack 1999). Unfortunately the resulting suppression is only effective for low baryon fractions, making it insufficient to account for observed luminosity functions given today’s concordance Λ CDM parameters (Benson et al. 2003). A related possibility is offered by starvation of galaxies simply because accretion slows down at late times (Feldmann & Mayer 2015; Feldmann et al. 2016). However the host halo masses of red galaxies are observed to be systematically lower than those of star-forming galaxies, suggesting that accretion continues after star formation shuts down (Mandelbaum et al. 2016). Semi-analytic models also suggest that without additional mechanisms, it is very difficult to quantitatively explain the division of the population into actively star-forming disks and “quenched”, red ellipticals (Baldry et al. 2004; Bower et al. 2006). This division appears to be in place even at high redshift (Ilbert et al. 2010; Brammer et al. 2011).

Environmental effects, especially in high-density group and cluster regions can strip an infalling galaxy of its gas reservoir which leads to a more natural bimodality (e.g. Quilis et al. 2000; Gómez et al. 2003; Boselli & Gavazzi 2006; van den Bosch et al. 2008; McCarthy et al. 2008; Bahé & McCarthy 2015). However,

arXiv:1607.02507v2 [astro-ph.GA] 14 Oct 2016

quenching also occurs outside of these environments (van den Bosch et al. 2008; Guo et al. 2009; Peng et al. 2010; Wijesinghe et al. 2012). We are therefore led to re-examine the role of feedback. One route to increasing the efficacy of stellar feedback at intermediate and high masses is to induce intense, compact starbursts through major mergers or violent disk instabilities (Dekel & Burkert 2014; Ceverino et al. 2015; Zolotov et al. 2015; Tacchella et al. 2016). However quenching in this scenario remains fairly gradual, with star formation declining over several gigayears (Zolotov et al. 2015), whereas a number of lines of evidence suggest that a significant fraction of early type galaxies are formed by much more rapid quenching (e.g. Thomas et al. 2005; Schawinski et al. 2014; Belli et al. 2015; Barro et al. 2016). Moreover, in this picture, quenching can be maintained over long time periods only in high-mass galaxies where the virial shock prevents rapid cooling of material accreted after the starburst event (White & Frenk 1991; Birnboim & Dekel 2003). By definition, quenching star formation for longer than the cooling time of halo gas requires an energy source other than stellar feedback.

Many studies suggest that the crucial input comes from active galactic nuclei (AGN) powered by central supermassive black holes; see, for example, Di Matteo et al. (2005); Hopkins et al. (2005); Bower et al. (2006); Croton et al. (2006); Sijacki et al. (2007); Di Matteo et al. (2008); Cattaneo et al. (2009); Johansson et al. (2009); Fabian (2012); Dubois et al. (2013, 2016) and references therein. AGN drive rapid outflows which can be directly observed in post-starburst galaxies (e.g. Tremonti et al. 2007; Rupke & Veilleux 2011), suggesting that black holes are able to suppress star formation by removing the supply of gas. Adding weight to the connection between a galaxy and its central black hole (BH) is the strong observed correlation between BH mass and stellar mass in the bulge (Cattaneo et al. 2009; Volonteri & Bellocq 2012; Kormendy & Ho 2013), which can be interpreted either as evidence that the BH and SF are fed from the same supply of cold gas; that feedback from BH regulates the star formation rate; or even, for low-mass galaxies, that feedback from SF regulates the BH accretion (Dubois et al. 2015). It is possible that the true explanation is a combination of all three effects. But whatever the regulatory role that BHs play, observations also show that AGN activity is common in highly star-forming galaxies (e.g. Nandra et al. 2007; Simmons et al. 2012; Mullaney et al. 2012; Rosario et al. 2012, 2013; Förster Schreiber et al. 2014; Mullaney et al. 2015; Carniani et al. 2016), suggesting that the precise role of the BH is strongly dependent on other, unidentified factors.

In this paper, we will identify those factors by studying the interaction between AGN feedback and mergers in a realistic cosmological environment, discussing how it can lead to quenching that is maintained for periods longer than the halo cooling time. To address this question we require an approach that offers control over environment, accretion history, and feedback models. The basis for our study is a $z = 2$ galaxy with a dynamical mass of $10^{12} M_{\odot}$, simulated using the CHANGA code (Menon et al. 2015). Uniquely, we are able to modify the accretion history of the system by making minimal modifications to the large-scale structure. This ability to “genetically modify” the system that we study, while keeping the cosmological conditions consistent with the Λ CDM inflationary scenario, is introduced by Roth et al. (2016). Our main aim here is to study how the BHs respond to changing the significance of the most major merger. The combination of being able to control feedback and history with a fixed local environment (including the precise directions of the filaments that feed cool gas to the galaxy) allows us to isolate and identify the conditions required

for quenching. In particular, all simulations are run first with and then without BHs to quantify the effect of the AGN feedback.

This paper is structured as follows. In Sec. 2 we describe the simulations in more detail. The results are discussed in Sec. 3. Finally we conclude in Sec. 4.

2 SIMULATIONS

2.1 The genetic modification approach

The morphology and colour of a galaxy is determined jointly by its mass, environment and history in tandem with internal feedback processes. Idealised simulations allow one to study the collision of two isolated galaxies, and consequently form part of the existing evidence that black holes and mergers have a role to play in quenching (e.g. Di Matteo et al. 2005; Johansson et al. 2009). However, such a computational approach lacks a cosmological environment and so neglects the inflowing gas filaments that provide fresh material for star formation; the results show whether feedback is able to disrupt the existing cold gas content but do not address the galaxy’s evolution after this point. Conversely, traditional cosmological simulations include the interaction between a black hole and continuing gas accretion (e.g. Dubois et al. 2013; Choi et al. 2015), but do not allow one to build a predictive understanding of the dependence on merger history.

In this work we combine the best features of the two approaches: we study the interplay between mergers and BH feedback by using the genetic modification (GM; see Roth et al. 2016) approach to generate a series of closely-related initial conditions which lead to different accretion histories. Our three initial conditions share the same large-scale structure and power spectrum, allowing us to make a controlled study while maintaining features such as the filaments along which gas streams.

We start with an unmodified reference zoom cosmological simulation of a galaxy of virial mass $M_{\text{vir}} \simeq 10^{12} M_{\odot}$ (see Sec. 2.2 for cosmological and numerical parameters). The linear overdensity field on the initial grid is denoted by the vector δ_0 ; each particle in the simulation then maps to a particular element of this initial vector. To increase (or decrease) the significance of a particular merger, we identify the particles of the infalling substructure and increase (or decrease) their mean overdensity in the initial linear vector. To compensate the final mass, the mean overdensity of the elements mapping to the final halo at $z = 2$ must be kept fixed.

It is not possible to simply modify the δ_0 linear overdensity vector by hand, since this would typically make the resulting field an extremely unlikely draw from the Gaussian random ensemble. The Roth et al. (2016) approach chooses a modified field δ_1 that is as close as possible to the original δ_0 in the sense of minimising $(\delta_1 - \delta_0)^T \mathbf{C}^{-1} (\delta_1 - \delta_0)$ while also satisfying the imposed overdensity modifications¹. Here, \mathbf{C} is the covariance matrix generated from the Λ CDM power spectrum.

For the purposes of this work, we generated three versions of a galaxy in the same large scale structure but with differing merger histories. The specific modifications are described further in Sec. 2.3. We verified that our constraints lead to a field that is consistent with being drawn from a Λ CDM power spectrum by calculating

¹ We implement the field changes by extending the code described by Roth et al. (2016) to allow the spatially-varying resolution required for zoom simulations. The mathematical formalism does not change; the technical implementation will be described in a forthcoming paper.

that $\chi^2 \equiv \delta_1^\dagger \mathbf{C}^{-1} \delta_1$ remains close to N , the number of particles (i.e. degrees of freedom) in the simulation. In the modifications described below, $\Delta\chi^2 = \pm 2$, which is a small perturbation around the $N \simeq 1.9 \times 10^7$ degrees of freedom in the box. Since the modifications are concentrated in the zoom region, one might instead compare to $N \simeq 1.7 \times 10^6$ in the zoom region. Seen either way, the modifications produce a field that is strongly consistent with the Λ CDM power spectrum.

2.2 Running the simulations

The simulations are performed using the task-based parallelised Tree-SPH code CHANGA which uses a geometric mean-density SPH interpolation approach, reducing artificial surface tension to better resolve fluid instabilities (Menon et al. 2015). The physics implemented includes star formation, supernova feedback and metal cooling. We also include a new prescription for BH formation, accretion and feedback. One key recommendation from multiscale studies of accretion on multiple scales (e.g. Hopkins & Quataert 2010, 2011) is that angular momentum support plays a critical role in determining BH growth in disk galaxies (see also Rosas-Guevara et al. 2015; Anglés-Alcázar et al. 2016). Our accretion model is therefore based on a modified Bondi-Hoyle formula that accounts for the rotational support of gas on resolved scales without requiring additional sub-grid assumptions (Tremmel et al. 2016). Additionally our approach includes a dynamical friction prescription (Tremmel et al. 2015) that produces physically-motivated, resolution-independent predictions for BH trajectories and mergers.

Feedback from stellar winds, Type II and Ia supernovae, and black holes is deposited thermally in the SPH kernel surrounding the source. In contrast to the dynamics, the feedback is therefore explicitly resolution-dependent, reflecting that the physical processes underlying feedback are always unresolved and must be represented by an effective model. Accordingly we are left with a handful of numerical parameters; these are calibrated against the $z = 0$ luminosity function and BH – bulge-mass relation. The tuning procedure, and its verification using a $(25\text{Mpc})^3$ uniform resolution volume simulation known as ROMULUS25, is described by Tremmel et al. (2016). At present we have only calibrated the new feedback models at a single resolution, and we therefore adopt this resolution for the present work (see below). To isolate the effect of the BH feedback, we run each of our initial conditions twice; first including all forms of feedback (which we will refer to as a “BH+SNe” run), then again including only stellar feedback (“SNe-only”).

We assume a *Planck* Λ CDM cosmology throughout (based on Table 3, column 4 of Planck Collaboration 2015). We start by simulating a $z \simeq 2$ field galaxy with a quiet evolution history. In preparation, we performed a 50Mpc uniform volume dark-matter-only simulation, from which we selected halos with virial masses at $z = 2$ in the range $0.9 \times 10^{12} < M_{\text{vir}}/M_\odot < 1.1 \times 10^{12}$ with the intention of obtaining a galaxy of stellar mass $M_\star \simeq 5 \times 10^{10} M_\odot$. We eliminated objects within a comoving megaparsec of a more massive halo, leaving four candidates from which we picked the object with the smoothest accretion history. The biggest event in the halo’s history to $z = 2.0$ is a 1:5 merger at 1.7Gyr ($z = 3.7$).²

² Here, and throughout, we define merger ratios using the mass of bound dark particles as reported by Amiga’s Halo Finder (AHF, Knollmann & Knebe 2009) at the time that the infalling structure’s mass peaks.

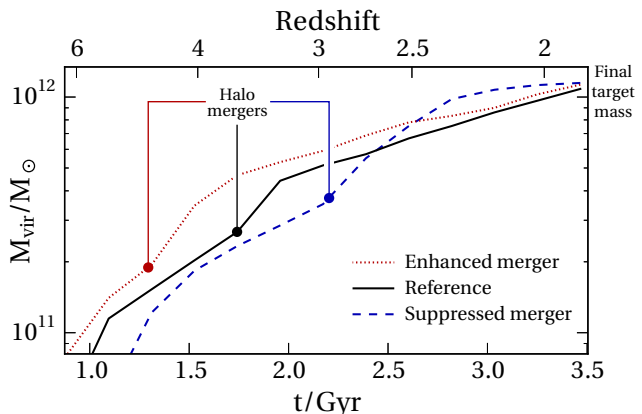


Figure 2. The virial mass over time of our three scenarios, showing the effect of the GM alterations. The black, red-dotted and blue-dashed lines refer to the reference, enhanced-merger and suppressed-merger runs in the SNe-only suite respectively. The build-up of mass differs, but by construction the final mass is fixed at the end of the simulations, $z = 1.8$.

At $z = 2.0$, the DM-only mass is $9.7 \times 10^{11} M_\odot$; by $z = 0.0$ this has grown to $3.3 \times 10^{12} M_\odot$.

We refined the density field around the target halo to generate zoom initial conditions (Katz & White 1993) and re-ran the simulation adding baryons. Our final simulation suite has a resolution of $M_{\text{p,gas}} = 2.1 \times 10^5 M_\odot$ and $M_{\text{p,dm}} = 1.4 \times 10^5 M_\odot$. (To achieve these similar particle masses, which is desirable to reduce noise in the potential near the centres of galaxies, the dark matter field is realised at twice the linear resolution of the gas field.) The Plummer-equivalent softening in the high-resolution region is 250 pc.

2.3 The merger histories

Using the GM approach (Sec. 2.1), we generate three different initial conditions; after running the simulations, we can study the corresponding three merger scenarios for our numerical experiment. The halo mass history is shown in Fig. 2. In summary:

- The original (“reference”) system’s largest merger prior to $z = 2$ has a mass ratio of 1:5 at $z = 4.0$ ($t = 1.5$ Gyr). Note that the galaxies merge slightly later than the parent halos, at $z = 3.2$ ($t = 2.0$ Gyr).
- Our first genetic modification is designed to generate a more significant merger by increasing the mass of the infalling object. This changed mass also causes the structure to fall in somewhat earlier; specifically we obtain a 2:3 merger at $z = 4.6$ ($t = 1.3$ Gyr; for the galaxies, $z = 3.7$ and $t = 1.7$ Gyr). We call this the *enhanced merger* simulation.
- Our second modification is designed to generate a smaller (but therefore later) merger. We found that due to the fixing of the final virial mass, it is accompanied by a rapid series of individually small accretion events that rapidly build mass (described below) around $z = 2.3$ ($t = 2.8$ Gyr; for the galaxies, $z = 2.5$ and $t = 2.6$ Gyr). We call this the *suppressed merger* simulation.

The top row of panels in Fig. 1 show the situation at $z = 3.0$ ($t = 2.2$ Gyr). At this time, the target halo has already merged in the reference and enhanced-merger scenarios (centre and right columns respectively). The large scale structure is therefore close to identical in the two cases, with only small changes in the positions of some individual objects. However at this time in the suppressed-

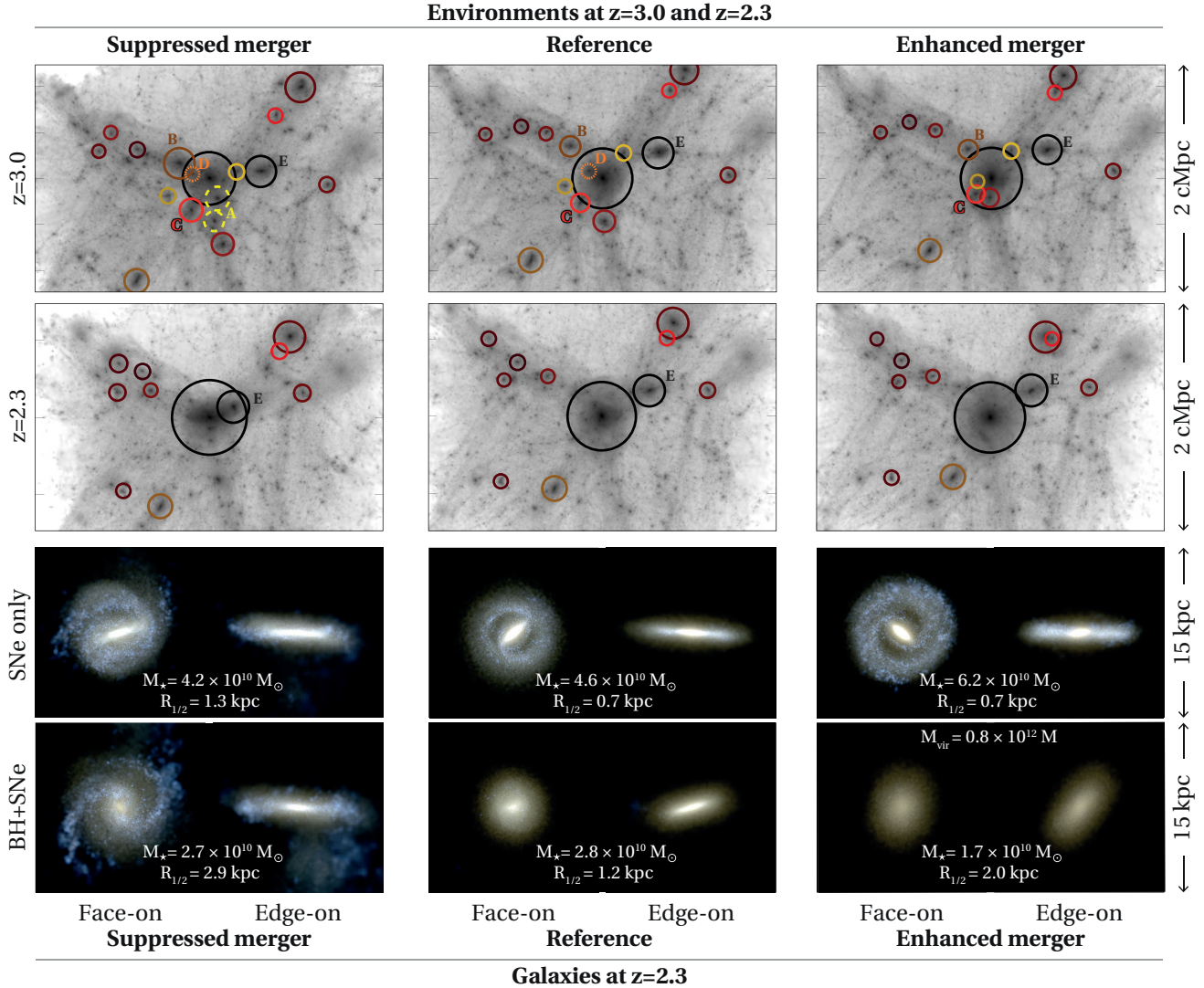


Figure 1. The genetic modification approach minimally changes the large scale structure while systematically altering the mass accretion history, to provide a controlled test of galaxy quenching. (*Upper two rows*) the projected density of dark matter in the high resolution region surrounding the SNe+BH galaxies at $z = 3.0$ and $z = 2.3$ respectively; the images are scaled to show dark matter column densities of 10^{19} to $10^{23} m_p \text{ cm}^{-2}$, where m_p is the proton mass. The most massive individual halos are identified by circles at the virial radii; halos are consistently labelled between the panels so that individual structures can be identified. Dotted/dashed halos have already merged into the main halo in the reference (A) and enhanced-merger (A and D) simulations. The significance of the other labelled structures is discussed in Sec. 2.3. (*Lower two rows*) portraits of the galaxy in UV rest-frame colours at $z = 2.3$ ($t = 2.8 \text{ Gyr}$, i.e. a lookback time of 11.0 Gyr). The images are scaled to cover a large dynamic range of 16 to 22 mag arcsec $^{-2}$. The upper of the two rows shows the SNe-only simulation suite; the galaxy forms a bright central bar/bulge. As our merger is made more significant and moved to earlier times, this becomes more concentrated. The bottom row depicts galaxies from the BH+SNe suite; the highly concentrated bars are absent, and the galaxy becomes increasingly quiescent, red and spheroidal as the merger ratio increases from left to right.

merger case (left column), the merger is just taking place. In fact the target merging substructure has actually been split into two halos, marked A. The uppermost of these halos is just about to merge with a ratio of 1:10, while the lower constitutes an additional minor merger of 1:25 at $z = 2.3$ ($t = 2.8 \text{ Gyr}$). The genetic modification, which targets a fixed $z = 2$ mass as an additional constraint, has partially compensated for the lower total mass present in accreted system A by increasing the mass of the separate infalling system B. This merges at $z = 2.5$ with a ratio 1:10 – whereas in the reference and enhanced-merger simulations the ratio for system B is 1:25 and 1:36 respectively. Meanwhile system C has a ratio of 1:20 and merges at $z = 2.5$ in all cases. Accompanied by a large number

of other even smaller substructures such as system D (1:60), the net effect is that the suppressed-merger halo grows rapidly around this time but without any major mergers.

In all three cases, system E tidally interacts with the main halo but is on a tangential trajectory and does not merge in the lifetime of our simulations. The closest approach occurs at $z \simeq 2.3$ ($t = 2.8 \text{ Gyr}$), illustrated in the second row of Fig. 1.

3 RESULTS

The lower panels of Fig. 1 show portraits of the galaxy in UV rest-frame colours at $z = 2.3$ in the three SNe-only runs (middle

row) and the corresponding SNe+BH runs (bottom row) with luminosity scaling between 16 and 22 mag arcsec⁻². Each simulation is shown in a face-on and edge-on projection, established according to the angular momentum of the baryons. The images are not dust-attenuated.

In the BH+SNe suite, the original and enhanced-merger scenarios give rise to a quenched, elliptical galaxy at $z = 2.3$. This is confirmed by analysis of the specific star formation rates (sSFRs), defined by $\text{sSFR} \equiv \dot{M}_*/M_*$ in Fig. 3. The first and second panels show the BH+SNe and SNe-only simulation suites respectively. We also calculate the main sequence star formation rate $\text{SFR}(M_*, z)$ using the fitting formula from Tomczak et al. (2016), itself based on ZFOURGE³ supplemented by far-infrared observations from *Herschel* and *Spitzer*. The result is plotted with ± 0.5 dex scatter as grey bands. For the input stellar mass M_* we use the reference simulation (noting that the sensitivity of the sSFR to M_* is relatively weak). It can be observationally convenient to define a quenched galaxy by its locus in the rest-frame UVJ colour plane (e.g. Williams et al. 2009; Whitaker et al. 2011); this results in an upper limit on the specific star formation rate of approximately $2 \times 10^{-10} \text{ yr}^{-1}$ (e.g. Domínguez Sánchez et al. 2016), which is shown as a horizontal line in Fig. 3.

In the SNe-only suite, the merger history has a relatively small effect, with star formation remaining active in all three cases. However in the BH+SNe case (top panel of Fig. 3), the behaviour becomes highly sensitive to history. The remainder of this Section explores why the BH feedback is sensitive to accretion history, and especially why it leads to a rapid and long-term quenching in the enhanced-merger scenario at $t = 2.0$ Gyr. First, we will inspect the accretion rates of the BHs (Sec. 3.1) before showing that the coupling rather than the total amount of energy is the key differentiating factor of the BH+SNe suite (Sec. 3.2). Sec. 3.3 shows that the BH is required not just to initiate quenching but to sustain it. However we also show in Sec. 3.4 that the BH actively accretes in the suppressed-merger scenario; star formation is allowed to continue because the AGN is kept under control by the dense, rotation-supported gaseous galaxy disk. Sections 3.5 and 3.6 draw implications for the population of galaxies as a whole. Finally, in Sec. 3.7, we briefly consider the dynamical impact of the BH feedback.

3.1 Black hole accretion rates remain strongly sub-Eddington, even during mergers

Figure 4 shows three ways of quantifying the BH accretion rate over time in the three BH+SNe simulations. As before, reference, enhanced, and suppressed merger simulations are represented by black solid, red dotted and blue dashed lines. The top panel shows the total BH accretion rate \dot{M}_{BH} . In our prescription, which follows the physical orbit of BHs rather than tying them to the halo centre, there can be more than one BH per halo; at each timestep we therefore sum over all that are in the major progenitor halo. Nonetheless, we found that the total mass and the accretion rate are both strongly dominated by one central BH except for a few timesteps around mergers.

Note that the drop in accretion rate at $t \simeq 2.8$ Gyr in all three scenarios is linked to a strong tidal interaction at closest approach of Halo E (as shown in Fig. 1). While this modestly increases the central density, it also increases the significance of the angular momentum support term (Tremmel et al. 2016), so that the net effect is

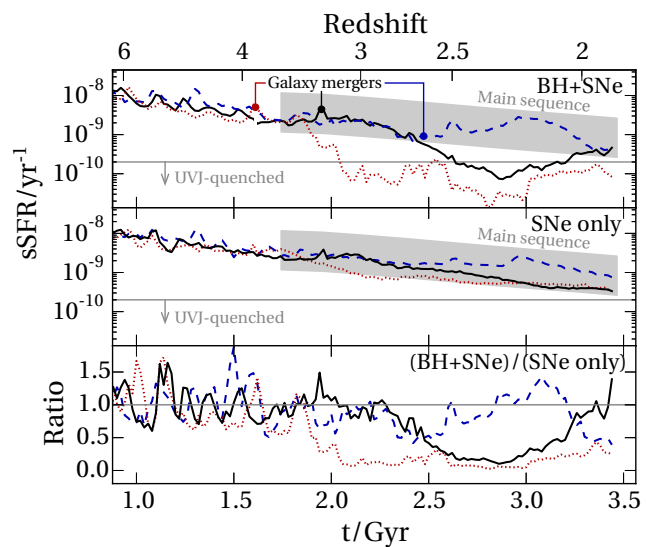


Figure 3. The interaction between BH feedback and merger history determines whether a galaxy quenches. *Top two panels:* The specific star formation rate (sSFR) of our three galaxies in the BH+SNe and SNe-only simulation suites respectively. Colours and linestyles correspond to those in Fig. 2. In the BH+SNe suite, the enhanced-merger case quenches permanently, the reference simulation quenches temporarily, and the suppressed-merger simulation never quenches. The grey band shows the approximate main sequence expectation using the fits from ZFOURGE supplemented by far-IR imaging (Tomczak et al. 2016) evaluated at the stellar mass of the reference galaxy. When galaxies fall below $2 \times 10^{-10} \text{ yr}^{-1}$ (horizontal lines), they are defined as quenched by the widely-used UVJ observational cut. *Bottom panel:* The ratio between the sSFRs of each merger scenario for the two different feedbacks, underlining how the relative effect of BH feedback is strongly dependent on history.

an overall reduction in the accretion rate. After the tidal event, the accretion rates recover. In the suppressed-merger case, the AGN becomes offset relative to the galaxy centre by 500 pc, leading to an increased accretion rate as its orbit decays. The consequences will be discussed in Sec. 3.4.

The middle panel shows the accretion rate \dot{M}_{BH} normalised to the star formation rate \dot{M}_* . The grey band represents the observed relationship averaged over many galaxies, $\langle \dot{M}_{BH} \rangle \simeq (0.6 \pm 0.1) \times 10^{-3} \langle \dot{M}_* \rangle$ at $z = 2$ (Mullaney et al. 2012). The redshift evolution of this relationship is extremely weak at least to $z = 3$ (Stanley et al. 2015), and so we have plotted a single mean relationship. Physically, the relationship is thought to derive from a common gas infall rate to the BH and stellar components (Dai et al. 2015; Harris et al. 2016); individual objects scatter significantly around the mean relation (Stanley et al. 2015), since this connection is imperfect.

The final panel of Fig. 4 shows the accretion as a fraction of the Eddington limiting rate, defined by $\dot{M}_{Edd} = 2.2 \times 10^{-8} \dot{M}_{BH} \text{ yr}^{-1}$ given the 10% radiative efficiency assumed by our BH implementation. The accretion rate averages 1.6% of Eddington, even during the merging and quench phases, with only occasional bursts reaching a maximum of 15%. This contrasts with some earlier works in which an Eddington-limited phase is invoked (e.g. Di Matteo et al. 2005; Sijacki et al. 2007, 2015); our lowered Eddington fractions are more consistent with constraints from the observed quasar population (e.g. Kelly et al. 2010; Nesvadba et al. 2011) where there is no evidence for enhanced accretion after mergers (Villforth et al. 2014). A major factor in the suppression in our simulations is the explicit inclusion of angular momentum

³ The FourStar Galaxy Evolution Survey, <http://zfourge.tamu.edu>

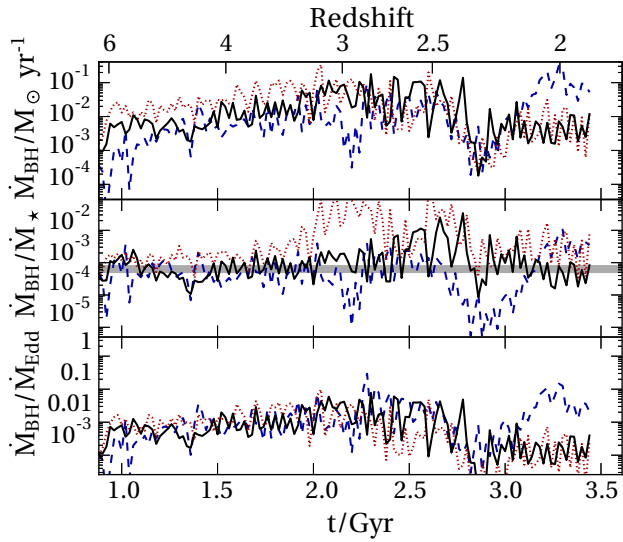


Figure 4. The BH feedback operates at a low Eddington ratio, even during mergers. From top to bottom, the total BH accretion rate is shown as an absolute rate, as a fraction of the star formation rate and as a fraction of the Eddington rate. Before quenching, all three galaxies closely conform to the mean observational relation from Mullaney et al. (2012) (grey band, middle panel). At later times, the luminosity of the BH is sustained and therefore increases as a fraction of the star formation rate. The tidal interaction with halo E (see Fig. 1) causes a drop in accretion rate in all three scenarios at $t \simeq 2.8$ Gyr followed by a slight rise in the suppressed-merger case, explained in the text.

support (Hopkins & Quataert 2011; Tremmel et al. 2016). In galaxies with a dense, rotationally-supported gas disk the accretion rates are reduced by factors up to 10 relative to a standard Bondi-Hoyle approach; the behaviour of the BH in different circumstances is discussed further in Sec. 3.4.

3.2 Energy coupling matters more than total energy input

The BH feedback is essential to quenching (Fig. 3); we now consider why the supernova feedback is unable to play this role. With our numerical parameters, the energy that couples thermally to gas for each solar mass accreted onto the BH is 3.6×10^{51} ergs, whereas the value for each solar mass of stars formed is 6.8×10^{48} ergs. Using the rates from Figs 3 and 4 respectively, we calculate the total energy deposited by all feedback sources in the SNe-only and BH+SNe suites. The top panel of Fig. 5 shows the energy injection accumulated over time $E_{\text{tot}}(< t)$ in the BH+SNe simulations as a fraction of that in the SNe-only equivalents. The ratio is approximately unity, and declines over time; in energetic terms, the reduced star formation rate in the BH+SNe simulations slightly overcompensates for the BH energy input.

The calculation above implies that total energy input is not the controlling factor deciding whether a galaxy quenches. Furthermore, Tremmel et al. (2016) showed that, in test runs, doubling the total energy input from supernovae is unable to reproduce the correct halo mass–stellar mass relation or the sSFR as a function of time; AGN have a qualitatively different effect to supernova feedback.

The lower panel of Fig. 5 focuses on the BH+SNe suite, showing the cumulative energy injected by BHs, $E_{\text{BH}}(< t)$, as a fraction of the total, $E_{\text{tot}}(< t)$. In the enhanced-merger case, 46% of the total

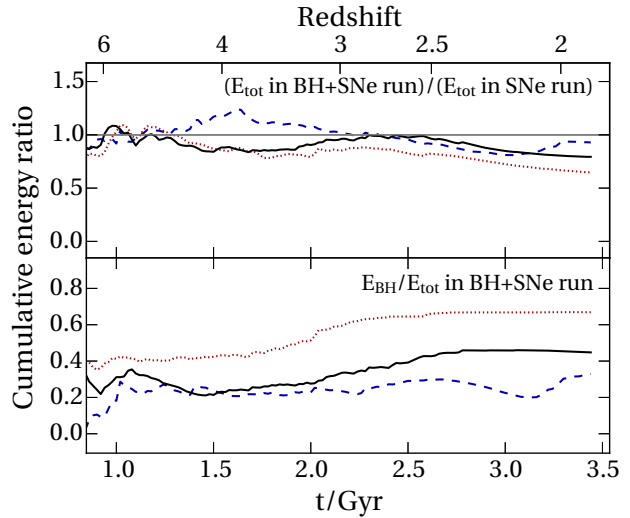


Figure 5. The total feedback energy input to the galaxies is approximately the same in BH+SNe as in SNe-only simulations. *Upper panel:* the total cumulative energy from all feedback sources in the BH+SNe runs as a fraction of the total energy in the SNe-only runs. In all three cases, the BH+SNe runs inject comparable feedback energy to the SNe-only runs. *Lower panel:* the fraction of energy delivered by the BHs in the BH+SNe suite. The BH energy input is significant in all cases, and dominates in the case of the enhanced-merger simulation. The balance between BH and SNe feedback determines whether large-scale outflows are generated.

feedback energy has been supplied by the BH at the time of quenching (1.8 Gyr), rising to 63% by the end of the simulation. The corresponding figures for the reference case are 42% (at quenching, 2.5 Gyr) and 43% (at the end of the simulation, by which time star formation has resumed and the fraction is falling). The cumulative contribution of BH feedback to the suppressed-merger case, which never quenches, does not exceed 35% at any time.

This strongly suggests a link between quenching and the fraction of feedback energy contributed by the AGN. To sharpen the connection, consider the energetics of gas leaving the galaxy (enclosed in a sphere at 10 kpc to be conservative). We calculate, for each particle i , the radial velocity $v_{r,i}$ and gas internal energy $u_i = 3kT_i/2m_p\mu_i$ (where k is the Boltzmann constant, m_p is the proton mass, T_i is the temperature and μ_i is the relative atomic mass of the gas). From here we define the outflow specific energy summary statistic as

$$\text{Outflow energy} \equiv \frac{\sum_i m_i v_{r,i} (u_i + v_{r,i}^2/2)}{\sum_i m_i v_{r,i}}, \quad (1)$$

where m_i is the particle mass and the sum is taken over all outflowing ($v_r > 0$) particles in the radial bin $9.5 < r/\text{kpc} < 10.5$. The expression (1) is constructed to give a specific energy representative of the bulk of the outflow, using a mean weighted by local outflow rate $v_r \rho$ where ρ is the local gas density.

Figure 6 shows the outflow specific energy defined in this way, divided by the specific energy required to overcome the gravitational potential, defined as $\Phi(r_{\text{vir}}) - \Phi(10 \text{ kpc})$. The upper and lower panels show BH+SNe and SNe-only suites. Values above unity (horizontal grey line) indicate that the majority of the outflowing gas is able to escape; conversely, values below unity imply that only a small proportion, if any, of the gas is able to escape the potential. We choose to plot against the virial mass of the halo (which monotonically increases with time) because, in the case of

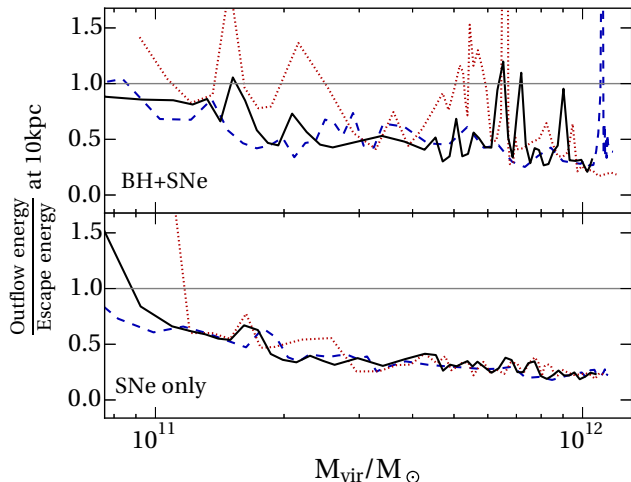


Figure 6. BHs are required for outflows at dynamical masses $M_{\text{vir}} > 10^{11} M_{\odot}$. The energy in outflows, defined by Eq. (1), is shown as a proportion of the energy necessary to escape the potential of simulated halos as they grow more massive over time. Independently of the assembly history, SN-generated winds (lower panel) are unable to leave the central regions of galaxies hosted in halos with mass approaching $10^{12} M_{\odot}$. On the other hand, BH feedback is centrally concentrated and therefore can create unbound winds at all halo masses (upper panel), even though the energy input is similar between the two simulation suites (Fig. 5).

supernovae, the outflow properties are then expected to be approximately independent of merger history (Keller et al. 2016).

The BH+SNe and SNe-only results are starkly different despite the two simulation suites invoking similar total feedback energy inputs (Fig. 5). The lower panel of Fig. 6 shows that supernova-driven outflows are increasingly ineffective at leaving the halo as the mass increases. This is consistent with the results of Christensen et al. (2016) who analysed the same SF prescription and found a mass outflow rate declining steeply with halo circular velocity. Conversely, the upper panel shows that BH feedback is able to eject gas from the halo at any mass.

We are now in a position to understand why BHs are essential to quenching. The BH feedback couples a significant fraction of the total available energy to a small mass at the very centre of the disk. This generates temperatures of order 10^7 K on the smallest resolved scales of a few hundred parsecs, while supernova bubbles rarely exceed 10^6 K. As the over-pressurised gas expands, the BHs give rise to high velocities but low gas densities in the centre of the galaxy; we find that typical mass outflow rates from the central kiloparsec are around 2 to 5 times *lower* in the BH+SNe suite.

There are two reasons why this low-mass, high-temperature feedback is more effective than supernovae by the time that we measure the outflow leaving the galaxy at 10kpc. First, the cooling time is longer; second, the total gravitational energy penalty for leaving the disk is lower. Both effects leave more of the feedback energy available for coupling to the halo gas. In the SNe-only suite, the mass outflow rates decline with radius as the gravitational and radiative energy losses cause the outflow to stall. Conversely in the BH+SNe cases, the mass outflow rates rise with radius because the initial energy losses are small and mass is swept up in an expanding shocked shell. It is this large-scale outflow, alongside the associated halo gas heating, that initiates and sustains galaxy quenching, as we now discuss.

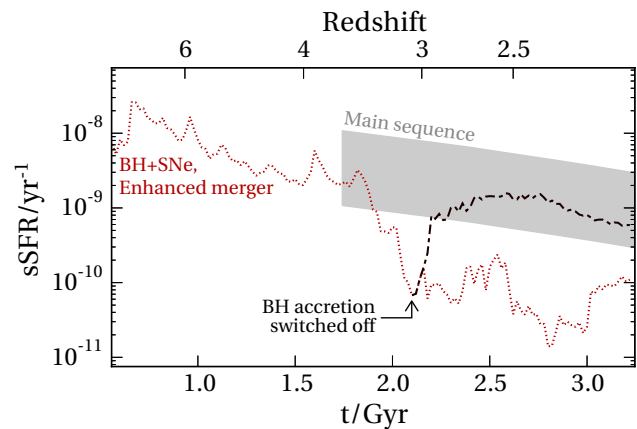


Figure 7. The BH is able to suppress star formation for periods much longer than the central cooling time (100Myr). As a test, we restarted the enhanced-merger BH+SNe simulation from $z = 3$ ($t = 2.17$ Gyr) with BH accretion artificially switched off, finding that the galaxy rapidly rejoins the main sequence by reforming a star-forming disk (black dash-dotted line).

3.3 The AGN is required to actively sustain quenching

The enhanced-merger BH+SNe simulation quenches for at least 1.5Gyr, to the end of the simulation. During this time, star formation rate drops by two orders of magnitude (Fig. 3) but the BH accretion rate remains steady (Fig. 4). Since the cooling time in the inner 10kpc of the halo is only 100Myr, this continuing feedback is crucial to maintaining the quenching (e.g. Croton et al. 2006; Sijacki et al. 2007). We directly verified that the BH energy input is required by restarting our enhanced-merger BH+SNe simulation from $z = 3.0$ ($t = 2.17$ Gyr), manually turning off the BHs after the sSFR has dropped to below 0.1 Gyr^{-1} . The results are shown in Fig. 7; star formation is rapidly re-established and the galaxy rejoins the main sequence in less than 200Myr. This underscores the importance of BHs to maintaining (as well as establishing) the quenched state.

It is worth investigating why the BH continues to accrete even when star formation cannot proceed, despite the two processes sharing a common fuel in the form of cooling gas. Figure 8 shows temperature maps of the gas in (top row) the enhanced and (bottom row) the suppressed-merger BH+SNe simulations. The left and right panels of each row show edge-on and face-on slices, as defined by the stellar angular momentum. First consider the quenched galaxy (top row). Crucially, there is cool ($\sim 10^4$ K) gas present which is able to feed the BH. Within 5kpc of the centre the total mass of neutral and molecular gas (which we do not distinguish in these simulations) is $1.2 \times 10^8 M_{\odot}$, compared to $4.0 \times 10^9 M_{\odot}$ in the SNe-only run. Observations indeed indicate that early type galaxies contain cold gas reservoirs in agreement with this result (e.g. Davis et al. 2014). The primary source of cool gas in both simulations is infalling streams.

When quenched, the turbulent remnant of the disk is able to rapidly remove angular momentum from new material. As a result, the greatest BH accretion rates are reached somewhat after the galaxy has quenched; the initial event involves mechanically disrupting the ordered rotation of the disk, after which the BH is able to cause substantial damage to the remaining cool interstellar medium. Observations show that BH activity can continue after star formation is shut off (e.g. Nandra et al. 2007), in agreement with this picture. Cool material that does not reach the central BH is typically disrupted by the rapid hot outflows in the vicinity.

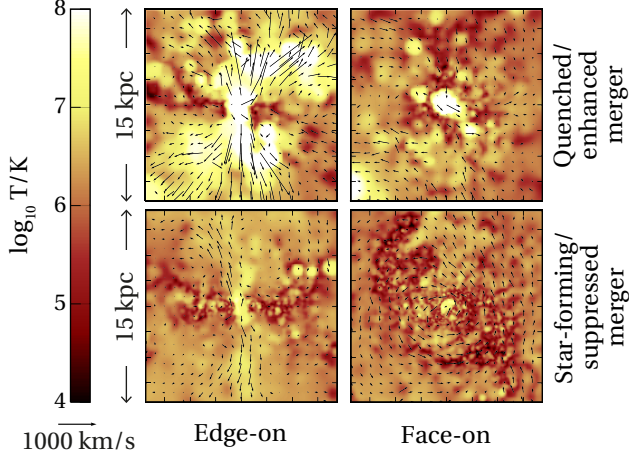


Figure 8. Temperature maps of the central 15 kpc show how the effect of the BH is strongly dependent on the gas around it. *Upper panels:* the enhanced-merger simulation shortly after quenching. The rotation-supported disk has been destroyed, replaced by a turbulent environment which can rapidly remove angular momentum from incoming cool material, maintaining BH accretion. *Lower panels:* The suppressed-merger simulation at the time of maximum star formation rate. Tidal forces have compressed the disk, but the angular momentum support restricts accretion onto the BH. Any energy released from the BH is strongly confined by the surrounding dense gas, so that it exits perpendicular to the disk and does not disrupt ongoing star formation.

Conversely in the star-forming mode (bottom row), infalling gas joins the ordered rotation of the disk, minimising the angular momentum losses. Once in a long-term stable orbit, the new gas fuels star formation. Our implementation of BH accretion includes the physical support provided by angular momentum on resolved scales (Tremmel et al. 2016), which limits the accretion rate even when the BH is surrounded by dense gas. Furthermore the effects of the feedback are confined by the presence of the disk, meaning that the star-forming regions are essentially shielded from any heating; the AGN energy is instead directed into the halo, perpendicular to the disk and cool gas inflow. This contrasts with the quenched system in which lack of pressure confinement for the BH feedback allows it to indefinitely prevent the re-formation of the disk.

The reference run serves as a helpful intermediate case where the cycle of quenching described above terminates (see Fig. 3): star formation resumes because the outer halo cools and provides enough dense gas to overwhelm the AGN feedback cycle. We investigate this more thoroughly below, after discussing how the suppressed-merger run avoids quenching entirely.

3.4 AGN activity can coexist with star formation

The suppressed-merger simulation never shuts off star formation; the rate peaks at $100 M_{\odot} \text{ yr}^{-1}$ at $t = 3.1 \text{ Gyr}$ and gently declines to $20 M_{\odot} \text{ yr}^{-1}$ at $t = 3.5 \text{ Gyr}$ (by which time it has a total stellar mass of $5.3 \times 10^{10} M_{\odot}$). We verified that, extending the simulation another timestep to $t = 3.6 \text{ Gyr}$, the galaxy remains on the star-forming main-sequence.

The peak in star formation rate is caused by the encounter with system E (Fig. 1). Closest approach occurs at $t = 2.8 \text{ Gyr}$; the tidal forces compress the gas disk and enhance star formation in both SNe and BH+SNe runs (Fig. 3). The enhanced, centrally concen-

trated star formation causes oscillation within the main sequence (Zolotov et al. 2015; Tacchella et al. 2016). As previously stated in Sec. 3.1, BH accretion rates also increase immediately following the tidal encounter, which drives a significant outflow for the first time in the history of the suppressed-merger galaxy. However the outflow is directed perpendicular to the disk which mitigates its impact on the instantaneous star formation rates, and the galaxy continues to be fuelled with fresh gas from the intergalactic medium (Fig. 9). The galaxy therefore does not quench; luminous AGN, star formation and rapid outflows can all coexist in the same galaxy, as seen in observations (Nandra et al. 2007; Förster Schreiber et al. 2014; Carniani et al. 2016).

3.5 The longevity of quenching depends on merger ratio

As discussed in Sec. 3.3, the enhanced-merger simulation with BH+SNe feedback quenches from shortly after the galaxies merge until the end of the simulation. However, the reference simulation quenches temporarily before reforming a star-forming disk. It rejoins the main sequence 1.5 Gyr after leaving it (Fig. 3); by the more stringent UVJ cut, the total period for which it appears quenched is less than 1 Gyr. At the end of the simulation it has a total stellar mass of $3.2 \times 10^{10} M_{\odot}$ and is forming new stars at a rate of $16 M_{\odot} \text{ yr}^{-1}$.

The difference between the two cases is understood by inspecting the rate of gas accretion into the galaxy (measured on a sphere at 10 kpc from the halo centre) as depicted in Fig. 9. The top two panels show the rate in SNe-only and BH+SNe suites respectively, with the bottom panel showing the ratio. In the reference and enhanced scenarios, BH feedback has the effect of reducing the accretion rate by up to a factor of two when the galaxies are quenched at $t = 2.5 \text{ Gyr}$. Conversely in the suppressed scenario, inflow rates are only weakly dependent on feedback – and, counter-intuitively, the average inflow rate is slightly higher in the BH+SNe case because some of the outflowing material is recycled in a galactic fountain. In the reference case, this fountain effect is seen after 3.0 Gyr: inflow compensates for the earlier BH-induced outflows. Such a compensation never occurs in the enhanced case over the lifetime of our simulation.

The three scenarios illustrate how the inflow rate depends critically on whether previously expelled material is able to cool or not. In the enhanced-merger case, the mean temperature of the circumgalactic medium at 150 kpc (measured at $t = 2.8 \text{ Gyr}$) is $T = 2 \times 10^5 \text{ K}$ in the enhanced-merger case, as opposed to $T = 0.8 \times 10^5 \text{ K}$ in the reference and suppressed-merger cases. This results in a cooling time at these radii of around 5 Gyr for the enhanced-merger case, contrasting with 1 Gyr in the other cases. Additionally, the cool inflowing material is easily disrupted in the more turbulent environment of the enhanced-merger simulation.

In summary, the reference simulation is able to regrow a disk because accretion continues and overwhelms the ability of the BH to expel material; conversely the enhanced-merger simulation maintains a lower accretion rate due to the higher initial energy input into the halo, uses the low level of accretion to directly fuel the BH, and consequently does not regrow its disk.

3.6 The fraction of quenched galaxies can be predicted

The discussion above explains how the enhanced-merger simulation, with a ratio of 2:3, quenches indefinitely whereas the reference (1:5) simulation quenches for $\sim 1 \text{ Gyr}$. In an attempt to refine the

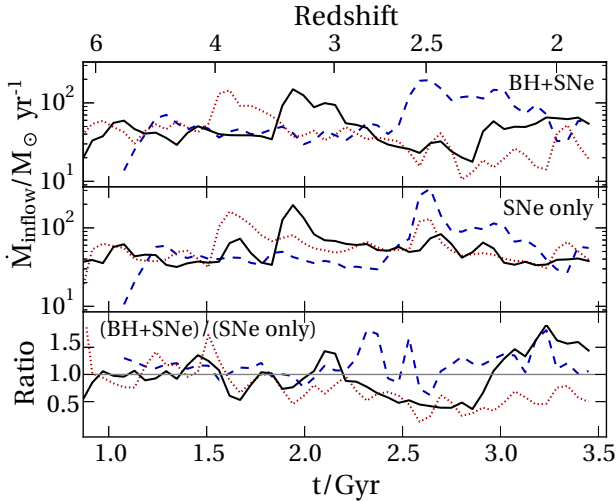


Figure 9. Long-term quenching requires the galaxy inflow to be suppressed. *Upper two panels:* The rate at which gas is inflowing across a fixed radius of 10kpc for BH+SNe and SNe-only suites respectively. *Bottom panel:* The ratio between the inflow in the two suites; accretion onto the galaxy is strongly suppressed for long periods by the BHs in the enhanced-merger case (red dotted line), but recovers at $t = 3$ Gyr in the reference case (black solid line). In the reference case, this leads to the reformation of the disk and readmission of the galaxy onto the star-forming main sequence, whereas the enhanced-merger galaxy never recovers (Fig. 3).

merger ratio required for long-term quenching, we ran an additional BH+SNe simulation that is intermediate between the reference and enhanced cases. We refer to the additional simulation as the *semi-enhanced* run. The ability to generate new cases to test hypotheses in this way is a major benefit of the GM approach (Sec. 2.1).

Figure 10 shows results from the semi-enhanced simulation (orange dash-dotted lines) alongside the reference and enhanced counterparts (solid black and dotted red lines). The halo merger in the semi-enhanced run takes place at $t = 1.6$ Gyr with a ratio of 1:3; the galaxies merge at $t = 1.8$ Gyr ($z = 3.5$). In the top panel, we show the specific star formation rate; like the enhanced case, the semi-enhanced run quenches shortly after its merger. The galaxy then weakly recovers its star formation between $t = 2.5$ Gyr and 2.7Gyr. This transitory effect results from a fountain-like recycling of the cool galaxy disk remnants. However the long-term galaxy accretion rate (lower panel) follows the enhanced-merger galaxy and so the star formation cannot be sustained.

Using the behaviour as a function of merger ratio, and tentatively adopting the assumption that this is the only variable determining whether a galaxy with a BH shuts off star formation or not, we can estimate the size of the quenched population. We take all halos from our dark-matter-only (50Mpc)³ simulation (Sec. 2) at $z = 1.8$ in the mass range $0.8 \times 10^{12} < M_{\text{vir}}/M_{\odot} < 1.2 \times 10^{12}$ (a total of 57 objects). We construct merger trees and find the largest merger event on the major progenitor branch for each of these halos up to $z = 4$, to match the merger events considered in this paper. Six halos (11%) have a merger at least as significant as 2:3; 15 (26%) more significant than 1:3 and 31 (54%) more significant than 1:5.

In a survey at $z \approx 1.8$, one can therefore expect roughly a quarter of all objects at $10^{12} M_{\odot}$ (or stellar masses of $\approx 3 \times 10^{10} M_{\odot}$) to be fully quenched, in agreement with observational estimates from a study of CANDELS 3D-HST fields (Lang et al. 2014). This picture predicts that a further quarter of objects in such a survey will

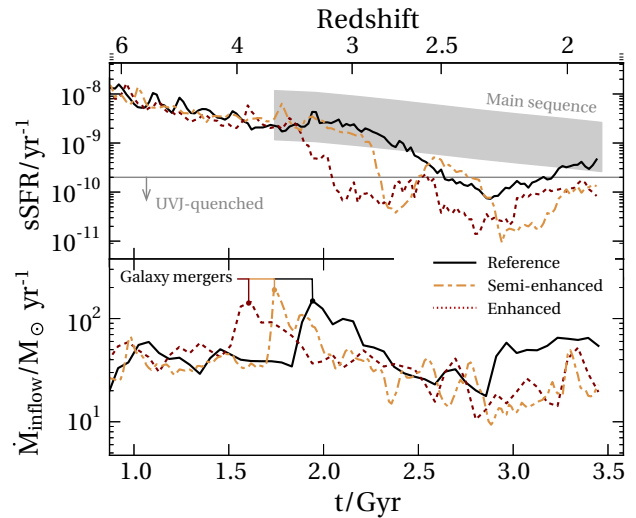


Figure 10. Using the genetic modification approach, we generate a semi-enhanced scenario in which the history is intermediate between the reference and enhanced-merger cases. The resulting galaxy has a 1:3 merger (as opposed to 2:3 and 1:5 for the enhanced and reference scenarios). *Upper panel:* The specific star formation rate of the new scenario with BH+SNe feedback (orange dash-dotted line). The enhanced (red dotted) and reference (black solid) cases are also plotted. The onset of quenching in the semi-enhanced case is intermediate between the two. Subsequently a fountain leads to some of the original disk reforming, although it is rapidly depleted. *Lower panel:* the inflow rate at 10 kpc for the three simulations. The times of the respective galaxy mergers are indicated. The semi-enhanced case suppresses inflow (and therefore long-term star formation) in the same manner as the enhanced simulation.

have quenched at some point in their past but subsequently “rejuvenated” and returned to the main sequence.

An attraction of working with the GM approach is that one can isolate different variables controlling a galaxy’s history and environment (see Sec. 4). Here we have worked on the hypothesis that major merger ratio is the most significant parameter; in future work we will discuss whether the predictions for quenched fractions remain robust when other aspects of a galaxy are allowed to change.

3.7 AGN activity prevents over-contraction of the dark halo

The ability of BHs to eject baryons from deep potential wells (Sec. 3.1) has knock-on effects on the overall dynamics of galaxies. The most direct consequence is that the central concentration of baryons is directly reduced, changing the rotation curve. Figure 11 shows the maximum circular velocity speed v_{max} (measured in the disk plane) as a function of time in each simulation. The BH+SNe suite forms galaxies with $v_{\text{max}} \approx 250 \text{ km s}^{-1}$ (top panel) whereas in the SNe-only suite (bottom panel), all galaxies reach $v_{\text{max}} = 500 \text{ km s}^{-1}$ which is unrealistically high (e.g. Wisnioski et al. 2015). The build-up of v_{max} over time in this SNe-only case closely tracks the gas accretion rate into the halo. When BH feedback is active, however, low angular momentum gas reaching the centre is efficiently ejected, so that growth of the galaxy’s v_{max} decouples from the total accretion even in the suppressed-merger case where the BH has relatively little impact on the overall star formation rate. AGN have also been shown to be critical for preventing over-contraction

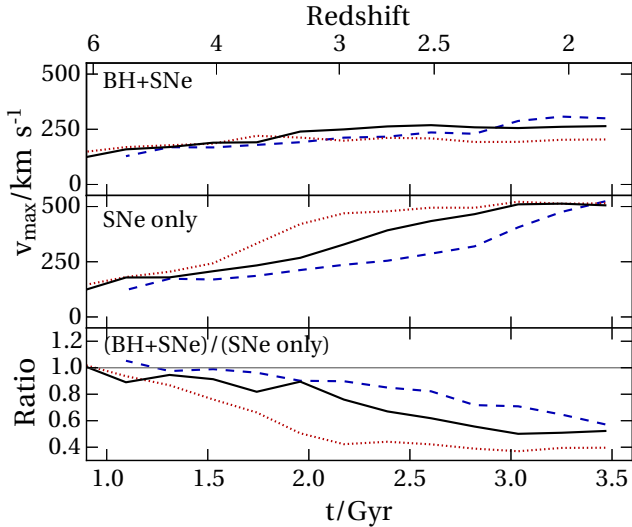


Figure 11. BHs regulate the build-up of baryonic mass in the centre of the galaxy. *Upper two panels:* The central concentration of baryons is quantified by measuring v_{\max} , the peak value of the rotation curve in the disk plane, for BH+SNe and SNe-only suites respectively. In the SNe-only case, v_{\max} continues to grow as mass accretes and falls into the centre, forming a bright central bar. In the BH+SNe case, a limit is reached at $v_{\max} \simeq 250 \text{ km s}^{-1}$. *Bottom panel:* The ratio of the simulations shows how AGN feedback at first has little effect on the dynamics, but as the BH mass grows, it becomes able to eject low angular-momentum material, preventing excessive central star formation.

of early-type galaxies at $z = 0$ (Martizzi et al. 2012; Dubois et al. 2013).

The dynamical time at the centre of our BH+SNe galaxies is approximately 100 Myr. Figure 4 shows that the BH accretion rate, and therefore energy input, varies on timescales considerably shorter than this period. According to the analytic arguments of Pontzen & Governato (2012), this should result in the expulsion of dark matter from the centre of the galaxy, and ultimately to the formation of a near-constant-density dark matter core (see also Martizzi et al. 2012; Pontzen & Governato 2014). For example, in the enhanced merger BH+SNe simulation, the limiting dark matter density profile (fitted in the innermost kiloparsec at $t = 3.5 \text{ Gyr}$) follows $\rho \propto r^{-0.7}$, which is significantly shallower than the $\sim r^{-1}$ scaling of a pure dark matter simulation. Conversely in the enhanced-merger SNe-only simulation, the same measurement gives $\rho \propto r^{-2.0}$, indicating a very strong adiabatic contraction from the dense pile-up of baryons. Our simulated BHs are therefore crucial in controlling not just the rate of star formation but the overall distribution of matter in the centre of galaxies.

The accretion of baryons and dark matter onto the halo is also affected by the BH feedback. The baryon fractions in the SNe suite remain at the cosmic mean fraction throughout the simulations, but strongly decline in the BH+SNe cases to 62%, 87% and 95% respectively⁴. This should have observable effects on the density of absorbers around early- and late-type galaxies (Suresh et al. 2015). The dynamics of the dark matter accretion are also affected,

⁴ However at the time of the most major merger, these differences are much smaller. The gas fraction of the infalling structure is 104%, 99.7% and 96.2% (105%, 103% and 104%) of the cosmic mean value in respectively the BH+SNe (and SNe-only) suite for suppressed, reference and enhanced cases.

since the reduction in gravitational mass slows subsequent accretion (Schaller et al. 2015). As only the BHs drive dynamically significant outflows, the BH+SNe galaxy halos have final dark matter masses that are 88%, 95% and 99.5% of the SNe-only masses for the enhanced, reference and suppressed-merger cases respectively.

4 CONCLUSIONS

In this paper, we investigated how galaxy mergers and black hole (BH) feedback work together to quench star formation. We used “genetically modified” initial conditions to set up three galaxies which live in the same environment and large scale structure, but that differ in merger history. Coupled to a new implementation of BH physics (Tremmel et al. 2016), we were able to isolate how mergers lead to quenching.

Our results show that quenching in field galaxies with virial masses larger than a few times $10^{11} M_{\odot}$ can only be achieved using BH feedback (Fig. 3). Supernova feedback becomes ineffective at driving galactic winds at these masses (Christensen et al. 2016; Keller et al. 2016). However the addition of BH feedback does not increase the total energy budget. Instead, its strong central concentration generates low-density outflows at high temperatures and velocities, minimising radiative energy losses. As the wind moves outwards, it sweeps up halo material, increasing the outflow density only after the deepest part of the gravitational potential has already been overcome. In this way the total energy loss due to purely gravitational effects is minimised.

Mergers trigger quenching without invoking a near-Eddington quasar phase for the central AGN. The average BH accretion rate agrees with constraints from stacking (Mullaney et al. 2012). All of our galaxies, regardless of the merger history, have an active BH at their centre, in keeping with observed AGN in both quenched and unquenched systems (Simmons et al. 2012; Mullaney et al. 2012; Rosario et al. 2015; Mancini et al. 2015), driving a large-scale galactic wind (Genzel et al. 2014; Harrison et al. 2014; Förster Schreiber et al. 2014). The cold disk of gas in the unquenched galaxies slows BH accretion due to angular momentum support. It also confines the effect of the BHs and directs it outwards in a funnel, allowing star formation to proceed despite the rapid central outflows (Cano-Díaz et al. 2012; Carniani et al. 2016).

Mergers start the quenching process through mechanical disruption of the cold disk. Subsequently the AGN feedback is able to have far greater impact in disrupting the existing star-forming gas and cool gas inflows. Acting together in this way, the merger and central BH push the galaxy into a self-sustaining, long-term quiescent state. The drop-off from the main sequence is rapid, occurring over around 250 Myr in both our reference and enhanced-merger simulations. Many clues suggest that quenching is indeed rapid in real galaxies (Barro et al. 2013, 2015; Mancini et al. 2015). In the simulations, quenching is followed by a slow decline in BH activity 0.5 – 1 Gyr after the galaxy leaves the main sequence, in agreement with observational evidence that AGN in star forming galaxies contribute the majority of the X-ray luminosity density (Mancini et al. 2015; Rodighiero et al. 2015). The quenching mode is then maintained by the turbulent remnants of the disk sweeping a low level of infalling cool gas into the BH, which allows BH accretion to continue as seen in recent observations by Tremblay et al. (2016). One prediction of this scenario is that quiescent galaxies will have an offset BH-stellar mass relation compared to star-forming galaxies (Terrazas et al. 2016).

The BH feedback has a significant dynamical impact on the

galaxy. Gas that is accreted into the disk at early times tends to carry little angular momentum; in the absence of a strong outflow or cycling mechanism, this piles up, creating a strong central bar (Fig. 1, third row of panels). The maximum circular speed in the disk plane reaches $v_{\max} \simeq 500 \text{ km s}^{-1}$ in all three merger scenarios when only stellar feedback is available (Fig. 11, top panel). The stronger outflows of the BH+SNe simulations prevent this pile-up from occurring, using a combination of a galactic fountain and outright ejection to set a limit of $v_{\max} \simeq 250 \text{ km s}^{-1}$. There is considerable interest in integral field spectroscopy of high-redshift galaxies (e.g. Förster Schreiber et al. 2006; Newman et al. 2015; Wisnioski et al. 2015), and we anticipate that the kinematics of galaxies can therefore be used as an indicator for the balance between BH and stellar feedback.

Our study hints at the broader potential of the “genetic modification” (GM) technique (Roth et al. 2016) to shed light on problems in galaxy formation. Because our three scenarios (reference, enhanced and suppressed) share the same environment and large scale structure (Fig. 1), with the central galactic disk assembling from gas streaming along the same filaments, we have been able to construct a clean test of the effect of merger ratio. The GM approach can search systematically over histories, providing controlled tests which retain the benefits of idealised simulations in pinning down the effect of merger ratio (e.g. Johansson et al. 2009) while also including cosmological accretion. We illustrated this point by constructing a scenario with a merger ratio intermediate between the reference and enhanced cases (Fig. 10). The results allowed us to estimate that a quarter of systems in our mass range at $z \simeq 2$ should appear quenched, and a further quarter will have recovered from an earlier episode of quenching – assuming that merger ratio is the significant variable controlling the outcome. Future work could extend this study by changing, for example, the mean density of the region within which the galaxy is hosted to directly interrogate the important role of environment (e.g. Peng et al. 2010; Wijesinghe et al. 2012).

ACKNOWLEDGMENTS

We are grateful to the anonymous referee for helpful comments. All simulation analysis made use of the PYNBODY (Pontzen et al. 2013) and TANGOS (Pontzen et al. in prep) suites. AP and AS were supported by the Royal Society. MT, FG and TQ were partially supported by NSF award AST-1514868. NR and HVP were partially supported by the European Research Council under the European Community’s Seventh Framework Programme (FP7/2007-2013) / ERC grant agreement no 306478-CosmicDawn. NR was additionally supported by STFC. MV acknowledges funding from the European Research Council under the European Community’s Seventh Framework Programme (FP7/2007-2013 Grant Agreement no. 614199, project “BLACK”). FG was partially supported by NSF AST-1410012, HST AR-14281 and NASA NNX15AB17G grants. This work used the DiRAC Complexity system, operated by the University of Leicester IT Services, which forms part of the STFC DiRAC HPC Facility (www.dirac.ac.uk). This equipment is funded by BIS National E-Infrastructure capital grant ST/K000373/1 and STFC DiRAC Operations grant ST/K0003259/1. DiRAC is part of the National E-Infrastructure.

References

- Anglés-Alcázar D., Davé R., Faucher-Giguère C.-A., Özel F., Hopkins P. F., 2016, preprint, (arXiv:1603.08007)
- Bahé Y. M., McCarthy I. G., 2015, MNRAS, 447, 969
- Baldry I. K., Glazebrook K., Brinkmann J., Ivezić Ž., Lupton R. H., Nichol R. C., Szalay A. S., 2004, ApJ, 600, 681
- Barro G., et al., 2013, ApJ, 765, 104
- Barro G., et al., 2015, preprint, (arXiv:1509.00469)
- Barro G., et al., 2016, ApJ, 820, 120
- Behroozi P. S., Wechsler R. H., Conroy C., 2013, ApJ, 770, 57
- Belli S., Newman A. B., Ellis R. S., 2015, ApJ, 799, 206
- Benson A. J., Bower R. G., Frenk C. S., Lacey C. G., Baugh C. M., Cole S., 2003, ApJ, 599, 38
- Binney J., 1977, ApJ, 215, 483
- Birnboim Y., Dekel A., 2003, MNRAS, 345, 349
- Boselli A., Gavazzi G., 2006, PASP, 118, 517
- Bower R. G., Benson A. J., Malbon R., Helly J. C., Frenk C. S., Baugh C. M., Cole S., Lacey C. G., 2006, MNRAS, 370, 645
- Brammer G. B., et al., 2011, ApJ, 739, 24
- Bullock J. S., Kravtsov A. V., Weinberg D. H., 2000, ApJ, 539, 517
- Cano-Díaz M., Maiolino R., Marconi A., Netzer H., Shemmer O., Cresci G., 2012, A&A, 537, L8
- Carniani S., et al., 2016, preprint, (arXiv:1604.04290)
- Cattaneo A., et al., 2009, Nature, 460, 213
- Ceverino D., Dekel A., Tweed D., Primack J., 2015, MNRAS, 447, 3291
- Choi E., Ostriker J. P., Naab T., Oser L., Moster B. P., 2015, MNRAS, 449, 4105
- Christensen C. R., Davé R., Governato F., Pontzen A., Brooks A., Munshi F., Quinn T., Wadsley J., 2016, ApJ, 824, 57
- Cole S., Aragon-Salamanca A., Frenk C. S., Navarro J. F., Zepf S. E., 1994, MNRAS, 271, 781
- Croton D. J., et al., 2006, MNRAS, 365, 11
- Dai Y. S., Wilkes B. J., Bergeron J., Omont A., Kuraszkiwicz J., Teplitz H. I., 2015, preprint, (arXiv:1511.06761)
- Davis T. A., et al., 2014, MNRAS, 444, 3427
- Dekel A., Burkert A., 2014, MNRAS, 438, 1870
- Di Matteo T., Springel V., Hernquist L., 2005, Nature, 433, 604
- Di Matteo T., Colberg J., Springel V., Hernquist L., Sijacki D., 2008, ApJ, 676, 33
- Domínguez Sánchez H., et al., 2016, MNRAS, 457, 3743
- Dubois Y., Gavazzi R., Peirani S., Silk J., 2013, MNRAS, 433, 3297
- Dubois Y., Volonteri M., Silk J., Devriendt J., Slyz A., Teyssier R., 2015, MNRAS, 452, 1502
- Dubois Y., Peirani S., Pichon C., Devriendt J., Gavazzi R., Welker C., Volonteri M., 2016, preprint, (arXiv:1606.03086)
- Efstathiou G., 1992, MNRAS, 256, 43P
- Efstathiou G., 2000, MNRAS, 317, 697
- Fabian A. C., 2012, ARA&A, 50, 455
- Feldmann R., Mayer L., 2015, MNRAS, 446, 1939
- Feldmann R., Hopkins P. F., Quataert E., Faucher-Giguère C.-A., Kereš D., 2016, MNRAS, 458, L14
- Förster Schreiber N. M., et al., 2006, ApJ, 645, 1062
- Förster Schreiber N. M., et al., 2014, ApJ, 787, 38
- Genzel R., et al., 2014, ApJ, 796, 7
- Gómez P. L., et al., 2003, ApJ, 584, 210
- Governato F., Willman B., Mayer L., Brooks A., Stinson G., Valenzuela O., Wadsley J., Quinn T., 2007, MNRAS, 374, 1479
- Guo Y., et al., 2009, MNRAS, 398, 1129

- Guo Q., White S., Li C., Boylan-Kolchin M., 2010, *MNRAS*, 404, 1111
- Harris K., et al., 2016, *MNRAS*, 457, 4179
- Harrison C. M., Alexander D. M., Mullaney J. R., Swinbank A. M., 2014, *MNRAS*, 441, 3306
- Hopkins P. F., Quataert E., 2010, *MNRAS*, 407, 1529
- Hopkins P. F., Quataert E., 2011, *MNRAS*, 415, 1027
- Hopkins P. F., Hernquist L., Cox T. J., Di Matteo T., Martini P., Robertson B., Springel V., 2005, *ApJ*, 630, 705
- Hopkins P. F., Kereš D., Oñorbe J., Faucher-Giguère C.-A., Quataert E., Murray N., Bullock J. S., 2014, *MNRAS*, 445, 581
- Ilbert O., et al., 2010, *ApJ*, 709, 644
- Johansson P. H., Naab T., Burkert A., 2009, *ApJ*, 690, 802
- Katz N., White S. D. M., 1993, *ApJ*, 412, 455
- Kauffmann G., White S. D. M., Guiderdoni B., 1993, *MNRAS*, 264, 201
- Keller B. W., Wadsley J., Couchman H. M. P., 2016, preprint, ([arXiv:1604.08244](https://arxiv.org/abs/1604.08244))
- Kelly B. C., Vestergaard M., Fan X., Hopkins P., Hernquist L., Siemiginowska A., 2010, *ApJ*, 719, 1315
- Knollmann S. R., Knebe A., 2009, *ApJS*, 182, 608
- Kormendy J., Ho L. C., 2013, *ARA&A*, 51, 511
- Lang P., et al., 2014, *ApJ*, 788, 11
- Mac Low M.-M., Ferrara A., 1999, *ApJ*, 513, 142
- Mancini C., Renzini A., Daddi E., Rodighiero G., Berta S., Grogin N., Kocevski D., Koekemoer A., 2015, *MNRAS*, 450, 763
- Mandelbaum R., Wang W., Zu Y., White S., Henriques B., More S., 2016, *MNRAS*, 457, 3200
- Martizzi D., Teyssier R., Moore B., Wentz T., 2012, *MNRAS*, 422, 3081
- McCarthy I. G., Frenk C. S., Font A. S., Lacey C. G., Bower R. G., Mitchell N. L., Balogh M. L., Theuns T., 2008, *MNRAS*, 383, 593
- Menon H., Wesolowski L., Zheng G., Jetley P., Kale L., Quinn T., Governato F., 2015, *Computational Astrophysics and Cosmology*, 2, 1
- Moster B. P., Naab T., White S. D. M., 2013, *MNRAS*, 428, 3121
- Mullaney J. R., et al., 2012, *ApJ*, 753, L30
- Mullaney J. R., et al., 2015, *MNRAS*, 453, L83
- Nandra K., et al., 2007, *ApJ*, 660, L11
- Nesvadba N. P. H., De Breuck C., Lehnert M. D., Best P. N., Binette L., Proga D., 2011, *A&A*, 525, A43
- Newman A. B., Belli S., Ellis R. S., 2015, *ApJ*, 813, L7
- Peng Y.-j., et al., 2010, *ApJ*, 721, 193
- Planck Collaboration 2015, preprint, ([arXiv:1502.01589](https://arxiv.org/abs/1502.01589))
- Pontzen A., Governato F., 2012, *MNRAS*, 421, 3464
- Pontzen A., Governato F., 2014, *Nature*, 506, 171
- Pontzen A., et al., 2008, *MNRAS*, 390, 1349
- Pontzen A., Roškar R., Stinson G., Woods R., 2013, pynbody: N-Body/SPH analysis for python, *Astrophysics Source Code Library* ([ascl:1305.002](https://arxiv.org/abs/1305.002))
- Quilis V., Moore B., Bower R., 2000, *Science*, 288, 1617
- Rees M. J., Ostriker J. P., 1977, *MNRAS*, 179, 541
- Rodighiero G., et al., 2015, *ApJ*, 800, L10
- Rosario D. J., et al., 2012, *A&A*, 545, A45
- Rosario D. J., et al., 2013, *ApJ*, 771, 63
- Rosario D. J., et al., 2015, *A&A*, 573, A85
- Rosas-Guevara Y. M., et al., 2015, *MNRAS*, 454, 1038
- Roth N., Pontzen A., Peiris H. V., 2016, *MNRAS*, 455, 974
- Rupke D. S. N., Veilleux S., 2011, *ApJ*, 729, L27
- Schaller M., et al., 2015, *MNRAS*, 451, 1247
- Schawinski K., et al., 2014, *MNRAS*, 440, 889
- Sijacki D., Springel V., Di Matteo T., Hernquist L., 2007, *MNRAS*, 380, 877
- Sijacki D., Vogelsberger M., Genel S., Springel V., Torrey P., Snyder G. F., Nelson D., Hernquist L., 2015, *MNRAS*, 452, 575
- Simmons B. D., Urry C. M., Schawinski K., Cardamone C., Glikman E., 2012, *ApJ*, 761, 75
- Somerville R. S., 2002, *ApJ*, 572, L23
- Somerville R. S., Primack J. R., 1999, *MNRAS*, 310, 1087
- Stanley F., Harrison C. M., Alexander D. M., Swinbank A. M., Aird J. A., Del Moro A., Hickox R. C., Mullaney J. R., 2015, *MNRAS*, 453, 591
- Suresh J., Rubin K. H. R., Kannan R., Werk J. K., Hernquist L., Vogelsberger M., 2015, preprint, ([arXiv:1511.00687](https://arxiv.org/abs/1511.00687))
- Tacchella S., Dekel A., Carollo C. M., Ceverino D., DeGraf C., Lapiner S., Mandelker N., Primack Joel R., 2016, *MNRAS*, 457, 2790
- Terrazas B. A., Bell E. F., Henriques B. M. B., White S. D. M., 2016, *MNRAS*, 459, 1929
- Thomas D., Maraston C., Bender R., Mendes de Oliveira C., 2005, *ApJ*, 621, 673
- Tomczak A. R., et al., 2016, *ApJ*, 817, 118
- Tremblay G. R., et al., 2016, *Nature*, 534, 218
- Tremmel M., Governato F., Volonteri M., Quinn T. R., 2015, *MNRAS*, 451, 1868
- Tremmel M., Karcher M., Governato F., Volonteri M., Quinn T., Pontzen A., Anderson L., 2016, preprint available on arXiv
- Tremonti C. A., Moustakas J., Diamond-Stanic A. M., 2007, *ApJ*, 663, L77
- Villforth C., et al., 2014, *MNRAS*, 439, 3342
- Volonteri M., Bellovary J., 2012, *Reports on Progress in Physics*, 75, 124901
- Whitaker K. E., et al., 2011, *ApJ*, 735, 86
- White S. D. M., Frenk C. S., 1991, *ApJ*, 379, 52
- White S. D. M., Rees M. J., 1978, *MNRAS*, 183, 341
- Wijesinghe D. B., et al., 2012, *MNRAS*, 423, 3679
- Williams R. J., Quadri R. F., Franx M., van Dokkum P., Labbé I., 2009, *ApJ*, 691, 1879
- Wisnioski E., et al., 2015, *ApJ*, 799, 209
- Zolotov A., et al., 2015, *MNRAS*, 450, 2327
- van den Bosch F. C., Aquino D., Yang X., Mo H. J., Pasquali A., McIntosh D. H., Weinmann S. M., Kang X., 2008, *MNRAS*, 387, 79